Modified surfatron device to improve microwave-plasma-assisted generation of RONS and methylene blue degradation in water

Juan Amaro-Gahete [a,b], Francisco J. Romero-Salguero [a], Maria C. Garcia [c,*]

[a] *Departamento de Química Orgánica, Instituto Químico para La Energía y El Medioambiente (IQUEMA), Facultad de Ciencias, Universidad de Córdoba, Campus de Rabanales, Edificio Marie Curie, E-14071, Córdoba, Spain*
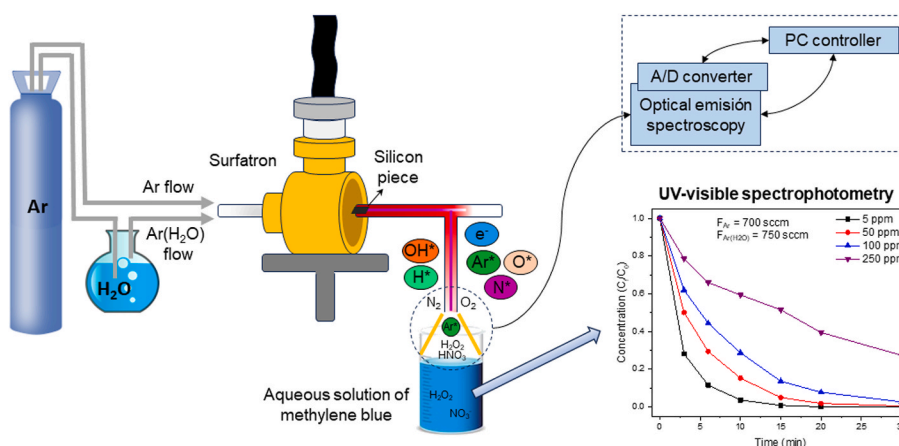[b] *Carbon Materials Research Group, Department of Inorganic Chemistry, Faculty of Sciences, University of Granada, Avda. de Fuente Nueva, S/n, Granada, ES18071, Spain*
[c] *Departamento de Física Aplicada, Radiología y Medicina Física, Universidad de Córdoba, Campus de Rabanales, Edificio Albert Einstein, E-14071, Córdoba, Spain*

HIGHLIGHTS

- A modified surfatron allows non-filamented plasma generation at lower power.
- The new plasma has a relatively high gas temperature and electron density.
- The plasma admits a high fraction of water, generating large amounts of OH.
- More reactive species form with the new surfatron configuration.
- Comparatively, this plasma shows a faster methylene blue degradation rate.

GRAPHICAL ABSTRACT

ARTICLE INFO

ABSTRACT

Microwave-induced plasmas generated at atmospheric pressure are very attractive for a great variety of applications since they have a relatively high electron density and can generate large amounts of reactive species. Argon plasmas can be sustained inside dielectric tubes but are radially contracted and exhibit filamentation effects when the diameter of the tube is not narrow enough (over 1.5 mm). In this work, we describe a new approach for creating microwave (2.45 GHz) plasmas under atmospheric pressure conditions by using a surfatron device and power from 10 W. This modified design of the reactor enables the sustenance of non-filamented argon plasmas. These new plasmas have a higher gas temperature and electron density than the plasma generated in the original surfatron configuration. The new design also allows for the maintenance of plasmas with relatively high proportions of water, resulting in the generation of larger quantities of excited hydroxyl radicals ($\cdot OH^*$). Thus, this novel configuration extends the applicability of microwave-induced plasmas by enabling operation under new conditions. Finally, the degradation of methylene blue (MB) in aqueous solutions has been assessed under

* Corresponding author.
E-mail address: fa1gamam@uco.es (M.C. Garcia).

different initial dye concentrations and argon flow conditions. The new plasma produces a substantial increase in hydrogen peroxide and nitrate concentrations in water and leads to a noteworthy enhancement in MB degradation efficiency. The introduction of water into the plasma produces a minor additional improvement.

1. Introduction

In the last fifty years, much theoretical and experimental work has been carried out on the fundamentals and applications of microwave-induced plasmas (MIPs), and their use has increased remarkably in various scientific and technological fields. Thus, these plasmas are being successfully employed in applications such as elemental analysis, surface treatment, illumination, the destruction of polluting gases, and sterilization (Calzada et al., 1992; Ferreira and Moisan, 1993; Hubert et al., 1986, 1979; Ilias et al., 2000; Kabouzi et al., 2003; Lebedev, 2015; Moisan et al., 1994; Moreau et al., 2000; Rezaaiyaan et al., 1987; Schelz et al., 1998). Microwave-induced plasmas can be generated under a wide range of experimental conditions: varying frequencies (200 MHz-20 GHz), different support gases (argon, helium, xenon, nitrogen, air, etc.), pressure conditions ranging from a few millitorrs up to various atmospheres, within dielectric tubes of various shapes and sizes or in an open environment via torch-type microwave coupling devices. Additionally, systems designed for generating these types of plasmas often incorporate additional energy coupling devices to maximize energy transfer from the source to the plasma, thereby optimizing their efficiency. These systems can also be equipped with reflected power meters to enable better real-time control of the power delivered to the plasma. Consequently, very stable, reproducible, and controllable microwave-induced plasmas can be sustained, making them an excellent choice for various applications, as these are qualities that not all types of plasmas have.

Microwave-induced plasmas sustained at atmospheric pressure are particularly attractive. They are non-thermal plasmas with a relatively high electron density and can generate large amounts of reactive species, thus exhibiting high reactivity. Furthermore, their generation under these pressure conditions simplifies the handling of MIPs, eliminating the need for complex vacuum systems.

Plasmas generated using argon as the feed gas have been widely studied and utilized, as this gas is relatively inexpensive and easier to ionize compared to other inert gases. Argon 2.45 GHz MIPs can be readily produced and sustained at atmospheric pressure using relatively low microwave powers (from ~30 W). Torch-type power coupling devices, such as TIA (Torche à Injection Axiale (Moisan et al., 1994)) and MPT (Microwave Plasma Torch (Jin et al., 1991)), generate argon plasma flames that are open to the air. TIA is commonly utilized to couple relatively high 2.45 GHz microwave power (up to approximately 2000 W), while MPT can only couple powers lower than 250 W.

Columnar argon plasmas can be maintained within dielectric tubes using surfatron and surfaguide-type devices (Ferreira and Moisan, 1993; Moisan and Pelletier, 1992; Moisan et al., 1987). At 2.45 GHz, these high-pressure plasma columns are radially contracted and do not entirely refill the tubes containing them (Castaños Martinez et al., 2004; Kabouzi et al., 2002). This radial contraction phenomenon is a characteristic of microwave discharges generated under specific experimental conditions with sufficiently high pressures, resulting in what is known as the filamentation effect, particularly notable at elevated feed-gas flow rates (Castaños-Martínez et al., 2009). This effect causes the plasma column to split into two or more smaller-diameter filaments, rendering it highly unstable. In order to prevent it, argon columns at 2.45 GHz and atmospheric pressure are usually produced in capillary tubes with a diameter smaller than 2 mm.

In this study, we present a novel procedure for generating atmospheric pressure 2.45 GHz non-filamented plasma columns within wide dielectric tubes by means of a surfatron device and using powers as low as 10 W. This new approach also facilitates the stable maintenance of

plasmas containing moderate fractions of water, thus enabling the generation of larger quantities of ·OH* radicals. The new configuration proposed in this work broadens the scope of applications for microwave-induced plasmas as new experimental conditions can be explored.

A comprehensive investigation into argon plasmas generated under various experimental conditions was conducted, also focusing on their capacity to produce reactive oxygen and nitrogen species (RONS) in aqueous environments. The generation of hydroxyl radicals, reactive species playing an outstanding role as promoters of Advanced Oxidation Processes, essential for water treatment (Foster et al., 2012; Foster, 2017; Stratton et al., 2015), is particularly interesting. In addition, this ability for RONS generation makes these non-thermal plasmas suitable for biomedical applications (Nastuta et al., 2011). Finally, we assessed the effectiveness of these plasmas in degrading methylene blue (MB) in aqueous solutions, considering different initial dye concentrations and plasma flow conditions, and conducted comparative analyses with other plasma reactors.

The increasing presence of organic pollutants, such as organic dyes, volatile organic compounds, and pharmaceuticals, in water resources poses a significant threat to the environment, ecosystems, and human health. Consequently, it is urgent to seek innovative remediation technologies tackling the removal of these toxic substances not addressed by conventional water treatment. Over recent years, non-thermal plasmas have emerged as a promising technology for water remediation (Aggelopoulos, 2022; Foster et al., 2012; Foster, 2017; Foster and Garcia, 2022; Magureanu et al., 2021). Indeed, in its interaction with water, these plasmas initiate Advanced Oxidation Processes (AOPs) that ultimately lead to the degradation and mineralization of pollutants. Plasma-generated species including excited atoms and molecules, charged particles, radicals, and UV radiation, among others, are responsible for driving these AOPs.

Different types of plasmas have been used for this purpose, including dielectric barrier discharges (DBD), corona discharges, gliding arcs, RF-plasma jets, and AC-needle plasmas, to mention just a few, as documented in recent comprehensive reviews (Aggelopoulos, 2022; Foster, 2017; Foster and Garcia, 2022). In addition to the choice of plasma source, an essential aspect to consider in this research is the nature of the plasma-water interaction. Some reactors employ a plasma-over-liquid configuration, involving an indirect interaction where the plasma does not directly contact the water. This configuration often requires one of the electrodes to be submerged in water, resulting in both electrical current flow through the liquid and the eventual degradation of the submerged electrode. Plasma jets, as an alternative, offer indirect water treatment without generating electrical current in the liquid or requiring a return electrode, thus minimizing water contamination.

Conversely, discharges can be created directly within the water, fostering a direct plasma-liquid interaction, which may or may not be mediated by the formation of bubbles. In a previous study (García et al., 2017), we reported for the first time on the use of a microwave (2.45 GHz) plasma jet for water remediation and designed a reactor with a plasma-over-liquid configuration that involved remote exposure of liquid samples. In our present work, we present a reactor with a similar plasma-over-liquid configuration but using plasmas with different characteristic parameters, in terms of electron density, gas temperature, and densities of excited reactive species.

2. Experimental section

2.1. Plasma reactor

Fig. 1 shows a schematic of the experimental setup used for plasma generation. A surfatron device was used to couple energy coming from a microwave (2.45 GHz) power supply (Microtron 200, with a maximum stationary power of 200 W in continuous-wave mode) to a support gas (argon) within a quartz tube of 6 and 8 mm of inner and outer diameter, respectively. Notably, this setup utilized relatively low microwave power levels, starting at 10 W. To achieve this, the usual electromagnetic field configuration created by the surfatron was altered by introducing a small rectangular Si(100) wafer (4 mm × 30 mm × 300 μm) into the discharge tube, as illustrated in Fig. 1a. In this way, a strong electric field established at the front edge of the silicon strip, resulting in the formation of an extended and stable plasma column, as illustrated in Fig. 1b. It is noteworthy that in this reconfigured setup, the plasma only formed in the region ahead of the silicon strip. In contrast to conventional surfatron experiments (Calzada et al., 1996; García et al., 2005), no plasma was observed within the surfatron region itself. Interestingly, in this newly conceived configuration, the phenomenon of plasma filamentation, which is a characteristic of microwave plasmas when sustained at atmospheric pressure in non-capillary tubes, did not occur, as depicted in Fig. 1b. Additionally, this configuration allowed for a reduction in the minimum power requirement for maintaining a stable plasma, decreasing from 30 W to 10 W.

Additionally, the new surfatron configuration facilitated the stable maintenance of the discharge, even when moderate quantities of water were introduced into the main gas stream, thus promoting the generation of ·OH reactive species in this type of plasma and enhancing its oxidative capability (*vide infra*).

In all experiments, a set of movable stubs allowed for impedance matching, thereby optimizing energy coupling to the extent that reflected power back to the generator became negligible (<5%).

2.2. Methods

In this work, the microwave power was set at 105 W, which allowed the generation of relatively long plasma columns ending near the open end of the tube, as depicted in Fig. S1. Argon was employed as the feed gas with its flow rate adjusted (using a calibrated mass flow controller) to $F_{Ar} = 700$ sccm (standard cubic centimeters per minute) in a primary gas line. To enhance the generation of ·OH species of this microwave plasma, a secondary argon feed line bubbling through water was also set. Various argon flow rates, denoted as $F_{Ar(H2O)}$, were employed, specifically 750, 1050, and 1550 sccm corresponding to 52, 60, and 69% of the total argon flow rate in each respective case. Assuming water saturation in this argon line, the volume percentage of H_2O in the feed gas (combining both primary and secondary lines) was 1.55, 1.80, and 2.07%, respectively, for the three $F_{Ar(H2O)}$ values. Fig. S1 shows what this plasma looks like. Here the tube design includes a vertical outlet to facilitate liquid treatment. As $F_{Ar(H2O)}$ increased, the plasma length experienced a slight and progressive shortening (from 2.8 to 2.5 cm). Compared to the conventional surfatron configuration, the new one enabled the stable maintenance of argon plasmas with significantly higher water content. Indeed, in the original configuration, $F_{Ar(H2O)}$ was limited to no more than 10% of the total argon flow rate, in contrast to the new configuration, which permits levels of up to 100%.

The plasma effluent downstream was directed into 8.3 mL of deionized water. The distance between the end of the plasma column and the water surface was about 4 mm at the beginning of the experiment. Consequently, the sample never came into direct contact with the plasma but instead underwent remote exposure to it. On the other hand, 8.3 mL solutions of methylene blue (MB) dye solutions, with varying concentrations (5, 50, 100, and 250 mg L^{-1}), were also treated.

Due to the relatively high gas temperatures and flows in the plasma, long exposure times enhanced the evaporation of the aqueous sample. All changes in the volume of the samples were considered for the quantification of the final concentration values.

2.3. Chemicals

Methylene blue dye (MB) was purchased from Sigma-Aldrich and used without further purification. The abatement of this stable heterocyclic aromatic compound belonging to the phenothiazine family ($C_{16}H_{18}N_3SCl$) has been extensively studied in recent decades due to the high environmental toxicological impact generated in MB-laden wastewater (Khan et al., 2022; Oladoye et al., 2022).

2.4. Analysis

In this study, Optical Emission Spectroscopy (OES) techniques (no invasive tools), were employed to diagnose the plasmas generated in the modified system. Fig. 1a also depicts the schematic of the optical detection assembly and data acquisition system utilized for processing OES measurements. A Czerny-Turner type spectrometer of 1 m focal length (Jovin-Yvon THR1000), equipped with a 1200 grooves/mm holographic grating and a photomultiplier (R636 Hamamatsu) as a detector, was employed to analyse the emissions from the plasma. This emission was side-on collected using an achromatic lens and an optical
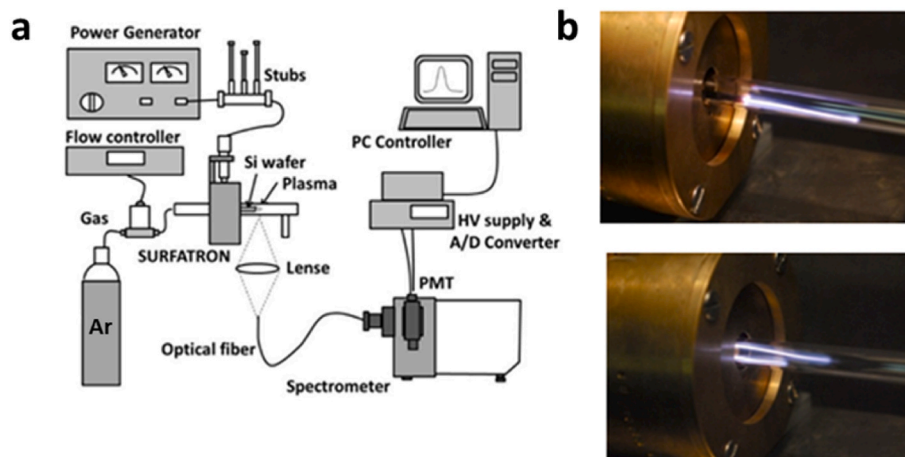

Fig. 1. a. Experimental set-up. Fig. 1b. Details of the argon plasma generated using both the new surfatron configuration (**up**) and the original surfatron configuration (**down**).

fiber and recorded with a spectral resolution ranging from 0.028 to 0.11 nm. HORIBA SynerJY™ software was used for spectra recording (integration time of 0.5 s). Analysis of the emission spectra provided us with valuable information about different excited species in the plasma that may have come into contact with the water and allowed us to determine the gas temperature and electron density in the plasma under the different experimental conditions investigated in this work.

The gas temperature (T_g) was measured from the collisional broadening of Ar I 840.82 nm emission line following the method proposed by Rodero and García in reference (Rodero and García, 2017). On the other hand, the electron density (n_e) was measured from the Stark broadenings of H_β line (atomic hydrogen Balmer series line), following the procedure described by Yubero et al. (2005). In this determination, the van der Waals contribution to the line profile was considered. Details about this method are included in the Supplementary section.

The formation of hydrogen peroxide, nitrate, and nitrites upon plasma treatment of deionized water was also examined. Peroxide-test strips (Quantofix, Peroxid 25, 0.5–25 mg L^{-1} Macherey-Nagel) and test strips for nitrate (10–500 mg L^{-1}) and nitrite (1–80 mg L^{-1}) from Macherey-Nagel were used for this purpose.

The degradation of the Methylene Blue (MB) dye through plasma exposure was assessed using UV–visible absorption spectroscopy in accordance with the work previously reported by our group (García et al., 2017) based on the research of Foster et al. (2013). UV–visible absorption spectra of the MB solutions were recorded at different time intervals of plasma treatment, using a PerkinElmer Lambda 650 S UV/Vis spectrophotometer in the wavelength range 250–800 nm. The conversion, referred to the percentage of MB degraded over the course of plasma treatment time, was calculated as (Eq. (1)):

$$conv\ (\%) = \frac{C_0 - C_f}{C_0} \times 100 \tag{1}$$

where C_0 and C_f are initial and final concentrations of the MB solution, respectively.

The apparent kinetic constant (k) was obtained by fitting to a pseudo first order reaction (Eq. (2)):

$$\ln\left(\frac{C_0}{C_f}\right) = k * t \tag{2}$$

where t is the reaction time (min).

Moreover, the energy yield defined as the ratio between the amount of MB removed during plasma treatment and the consumed energy was calculated following Eq. (3):

$$Energy\ yield\ \left(g\ kWh^{-1}\right) = Y = \frac{V\ (L) * C_0\left(g\ L^{-1}\right) * conv(\%)}{P(kW) * t(h) * 100} \tag{3}$$

where V is the MB solution volume and P is the microwave power supplied.

3. Results and discussion

3.1. OES plasma characterization and plasma excited species

The plasma emission was measured from a small spot located at the bottom of the vertical plasma column, so close to the liquid. Fig. S3a shows a typical optical emission spectrum for a pure argon discharge at this (bottom) position. Tables S1 and S2 in Supplementary data summarize the emission lines and bands identified and their spectroscopic characteristics (NIST, 2023; Pearse and Gaydon, 1976). The dominant species generated in this pure argon plasma were excited argon atoms.
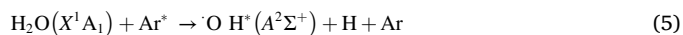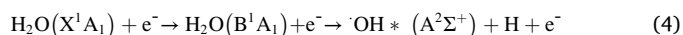
Qualitatively different spectra were observed for plasmas generated by adding some water (see Fig. S3b). In this case, the primary excited species were hydroxyl radicals and hydrogen atoms, while the emission from excited argon atoms experienced a significant reduction.

Additionally, we also recorded the spectrum emitted by the filamented plasma generated in the original surfatron configuration (i.e. without the silicon piece, Fig. S3c) to gain insight into the different properties of both types of discharges and infer the potential benefits of using the silicon piece. Regarding the excited species generated, this spectrum closely resembled the one emitted by the plasmas generated in the new configuration (with the silicon piece, Fig. S3a). However, as we will demonstrate later, there are notable differences between these plasmas in terms of their gas temperature and electron density.
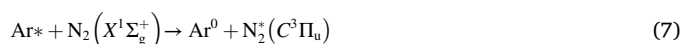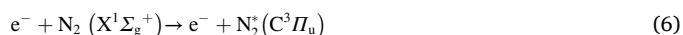
The presence of N$_2$*, NH*, and oxygen and excited nitrogen atoms in the spectra accounts for the intake of air into the discharge through the tube's end. It's worth noting that in the case of pure argon plasmas, ·OH* species stemming from ambient humidity (as a result of sample evaporation) were also identified.

Fig. 2 shows details on plasma emission under the different experimental conditions explored (flow rate variations while keeping the microwave power constant). As expected, the excitation of argon atoms exhibited a linear increase with the argon flow rate, owing to the higher argon content in the discharge. A similar trend was observed for the excitation of hydrogen and oxygen atoms resulting from water decomposition. Conversely, the population of nitrogen-containing excited species (N$_2$* and NH*) decreased with increasing argon flow rates. This decline was due to both the reduced presence of air in the tube at higher flow rates and the shorter residence times of these species in the plasma. The density of ·OH* excited species also increased with $F_{Ar(H2O)}$, although this change was relatively less pronounced.

The primary mechanism for generating ·OH*($A^2\Sigma^+$) is most likely water dissociation via impact reactions ($E_{threshold} \sim 10$ eV) involving either electrons or argon species (excited or metastable), as follows (Lu et al., 2016):

$$H_2O\left(X^1A_1\right) + e^- \rightarrow H_2O\left(B^1A_1\right) + e^- \rightarrow \cdot OH * \left(A^2\Sigma^+\right) + H + e^- \tag{4}$$

$$H_2O\left(X^1A_1\right) + Ar^* \rightarrow \cdot O\,H^*\left(A^2\Sigma^+\right) + H + Ar \tag{5}$$

On the other hand, the excitation of nitrogen molecules to $C^3\Pi_u$ state is likely produced from electron/Ar* collisions with nitrogen molecules at ground state $X^1\Sigma_g^+$ ($E_{threshold} = 11.08$ eV) through the following reactions (Britun et al., 2007; García et al., 2010; Lu et al., 2016; Yu and Yasuda, 1998):

$$e^- + N_2\left(X^1\Sigma_g^+\right) \rightarrow e^- + N_2^*(C^3\Pi_u) \tag{6}$$

$$Ar* + N_2\left(X^1\Sigma_g^+\right) \rightarrow Ar^0 + N_2^*(C^3\Pi_u) \tag{7}$$

Collisions of N$_2$* with molecular oxygen would be a source of oxygen atoms:
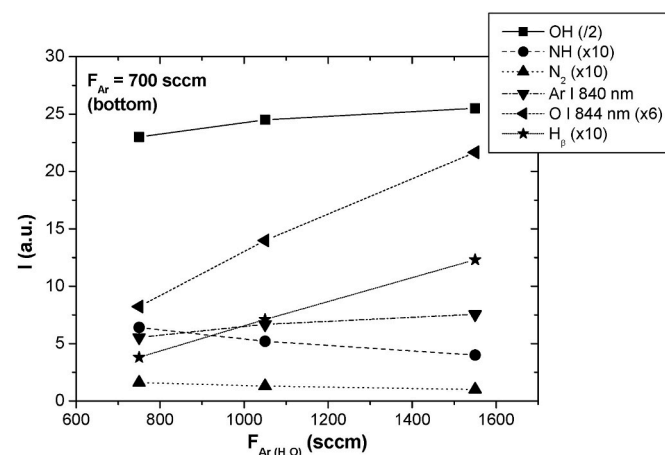
Fig. 2. Excited species in the plasma.

$$N_2^*\left(C^3\Pi_u\right) + O_2 \rightarrow N_2 + O + O \tag{8}$$

finally, the presence of species N* and NH* proved some N_2 dissociation in the discharge.

Fig. 3 (left) gathers the values of gas temperature (represented by circles) for each experimental condition explored in this work and measured from the collisional broadening of Ar I 840.82 nm emission line (Rodero and García, 2017). Notably, the gas temperature T_g exhibited a consistent increase with the humidified argon flow rate. Additionally, this figure includes the gas temperature of the plasma generated in the original surfatron design (represented by a star), with a total argon flow rate of 1450 sccm and no water fraction (as the plasma couldn't be sustained when introducing water). This temperature was significantly lower, consistent with the observation that, in this case, the plasma comprised two filaments, one horizontal and the other vertical, each of lower intensity compared to the single filament generated with the assistance of the Si piece. These filaments somehow shared the electromagnetic energy delivered by the surfatron. It's worth noting that the values of the rotational temperature derived from the simulation of the OH ($A^2\Sigma^+ \rightarrow X^2\Pi$) rotational band $T_{rot,OH}$ (represented by squares) are notably higher than T_g, clearly overestimating this plasma parameter.

On the other hand, Fig. 3 (right) depicts changes in the plasma electron density with $F_{Ar(H2O)}$. Increasing values of this parameter led to progressively higher values of n_e, ranging from 3.5 to $5.6 \cdot 10^{20}$ m^{-3}. We tentatively attribute these consistent increases of n_e and T_g with the humidified argon flow rate to better coupling of the energy to the plasma for higher $F_{Ar(H2O)}$. Notably, the electron density in the plasma generated with the original surfatron configuration (without Si piece), was also lower (ranging from $1.6 \cdot 10^{20}$ m^{-3} - $2.0 \cdot 10^{20}$ m^{-3}, for a total argon flow rate of 1450 sccm). In the new configuration, we produced microwave plasmas characterized by electron density and gas temperature distinct from those obtained using the original surfatron configuration. These results were not entirely unexpected, given that the original configuration was primarily intended for generating microwave plasmas sustained by surface waves, whereas plasmas created in the new design align more closely with the classification described by Lebedev in (Lebedev, 2015) as an 'electrode microwave discharge'.

3.2. Hydrogen peroxide, nitrate, and nitrite generated in water

Fig. 4 gathers the hydrogen peroxide and the nitrate generated in distilled water upon different plasma treatments. It is important to note that nitrites were not detected under any of the experimental conditions explored in this study. The results clearly indicate that the presence of

the silicon piece significantly enhanced the formation of both peroxides and nitrates. Fig. 4 (left) shows the existence of H_2O_2 species in water under all the plasma treatments investigated in this study, even in cases where no water was introduced through the secondary gas feed line ($F_{Ar(H2O)}$ = 0 sccm). In such cases, the only source of water was the sample being treated, and so ·OH* precursors involved in hydrogen peroxide formation must mainly come from water molecules evaporated from the sample. This mechanism must also contribute to H_2O_2 formation when some water was added into the discharge ($F_{Ar(H2O)} \neq 0$ sccm).

Interestingly, under the same total flow (1450 sccm), the production of H_2O_2 proved to be more efficient in the pure argon plasma (F_{Ar} = 1450 sccm + $F_{Ar(H2O)}$ = 0 sccm) than in the argon/water plasma (F_{Ar} = 700 sccm + $F_{Ar(H2O)}$ = 750 sccm). As previously mentioned, and shown in Fig. S3b, the excitation of argon species quenched upon introducing water into the plasma. This observation suggests that Ar* most likely plays a significant role in the H_2O_2 formation process through reactions (6) (García et al., 2017). In fact, the concentration of hydrogen peroxide exhibited the same increasing dependency on $F_{Ar(H2O)}$ (as well as the total argon flow rate) as that of Ar*, which further supports this hypothesis. Thus, taking into account the occurrence of sample evaporation, we tentatively propose that water dissociation in hydroxyl radicals and hydrogen atoms took place at the gas phase upon striking of argon excited species (including metastables) on water molecules in the gas phase through reactions (6), thus producing ·OH radicals. Subsequently, ·OH species react to produce hydrogen peroxide in the presence of a third molecule (Eq. (9)), and eventually, they solvate and diffuse into the bulk liquid (Eq. (10)) (Locke and Shih, 2011; Machala et al., 2019):

$$\cdot OH + \cdot OH + M \rightarrow H_2O_2 + M \tag{9}$$

$$H_2O_2 \rightarrow H_2O_{2,aq} \tag{10}$$

Also, ·OH species could have been solvated, and reactions (10) could have occurred in the liquid bulk (Machala et al., 2019).

Fig. S4 gathers the percentages of sample evaporation upon the different plasma treatments investigated in this study. Notably, when using the original surfatron configuration, the sample evaporation percentage was the lowest, aligning with the lowest T_g observed in this plasma. This correlation between the formation of H_2O_2 and the extent of water evaporation underlines, once again, the crucial role of evaporation in the generation of ·OH radicals.

On the other hand, Fig. 4 (right) shows that the formation of nitrates was more efficient for the case F_{Ar} = 700 sccm + $F_{Ar(H2O)}$ = 1550 sccm. It is well known that long-lived NO and NO_2 species generated at the gas phase serve as the precursor radicals for the formation of nitrites and nitrates in plasma-activated water (Lu et al., 2017). Indeed, after the
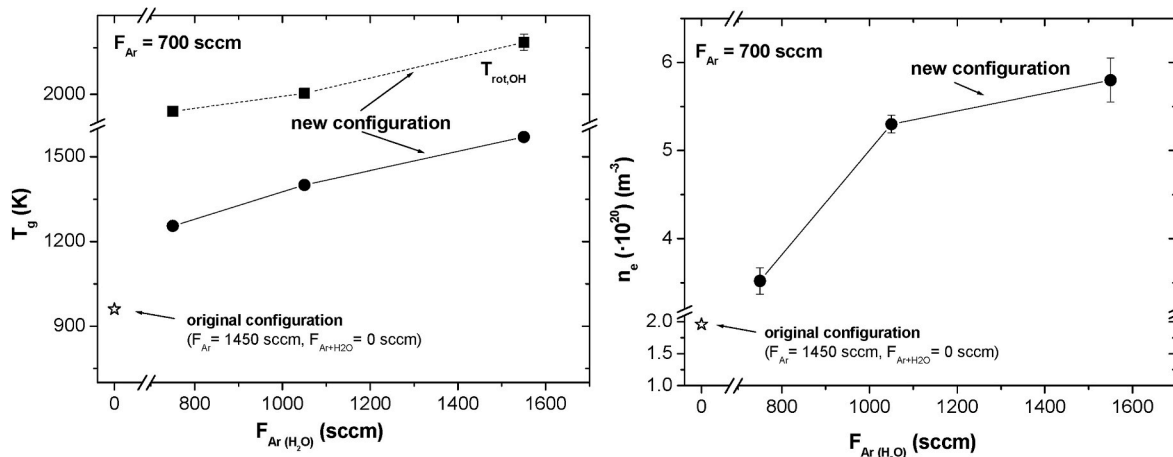

Fig. 3. Gas temperature (**left, circles**) and electron density (**right**) evolutions measured in the plasma generated in the new configuration and in the original one (stars). The squares in the graph represent the rotational temperature measured from the OH ($A^2\Sigma^+ \rightarrow X^2\Pi$) rotational band.
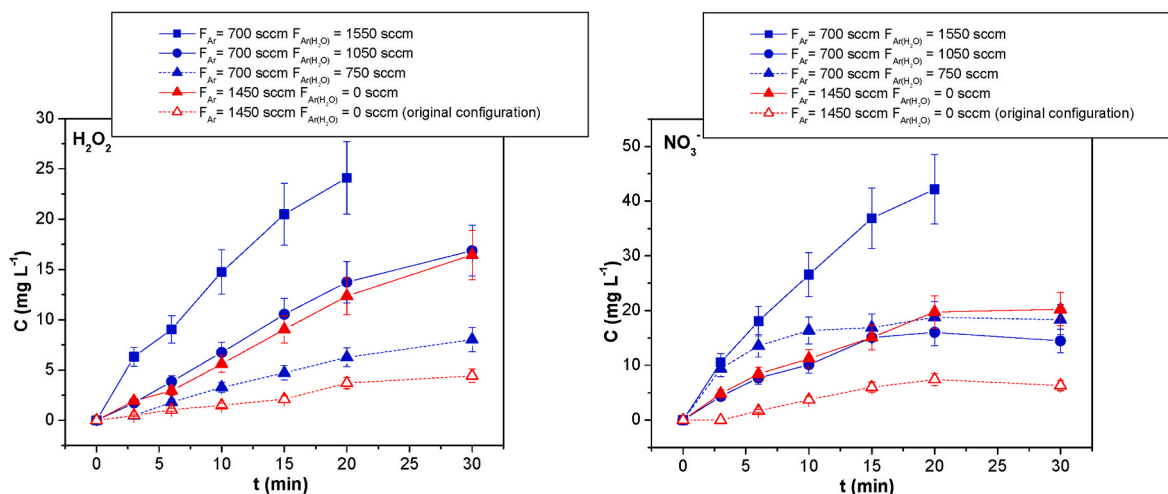
Fig. 4. Changes in concentrations of hydrogen peroxide **(left)** and nitrate **(right)** in deionized water after plasma treatment as a function of argon flow rate.

production of NO through Zeldovich mechanism, these species easily oxidize to NO_2. Eventually, reactions involving NO_2 and ·OH species generated in the gas phase would explain the presence of nitrates in treated water (Lietz and Kushner, 2016; Machala et al., 2019):

$$NO_2 + {}^{\cdot}O\,H \rightarrow HNO_3 \rightarrow HNO_{3,aq} \tag{11}$$

in this case, because the solubility coefficient of NO_2 is relatively small compared to that of hydrogen peroxide, reactions (11) are much less probable to occur in the liquid bulk.

As previously mentioned, nitrites were not detected under any circumstances. The high gas temperature in the discharge may have favored the formation of NO_2 (over NO formation) in the gas phase, resulting in a higher concentration of NO_3^-. On the other hand, the generation of peroxynitrous acid (O=NOOH) from the mixture of NO_2^- with H_2O_2 under acid conditions and the readiness of this acid to

decompose into NO_3^- would also account for the absence of nitrite in the treated samples (Lu et al., 2017). Fig. S5 depicts the evolution of pH and temperature of the water sample over time during the plasma treatment ($F_{Ar(H_2O)} = 750$ sccm and $F_{Ar} = 700$ sccm), confirming its acidification. Indeed, the pH experienced a progressive reduction from its initial value 7.02 to 2.92 after 20 min of plasma exposure.

3.3. Degradation of MB

The UV–visible spectra for plasma-treated MB solutions at different time intervals (ranging from 3 to 30 min) are represented in Fig. S6. These measurements were compared to an untreated MB solution at t = 0 min, with an initial dye concentration of 50 mg L^{-1}. The plasma used for the treatment was generated using a mixture of $F_{Ar} = 700$ sccm and $F_{Ar(H_2O)} = 750$ sccm. The spectra revealed a progressive reduction in the
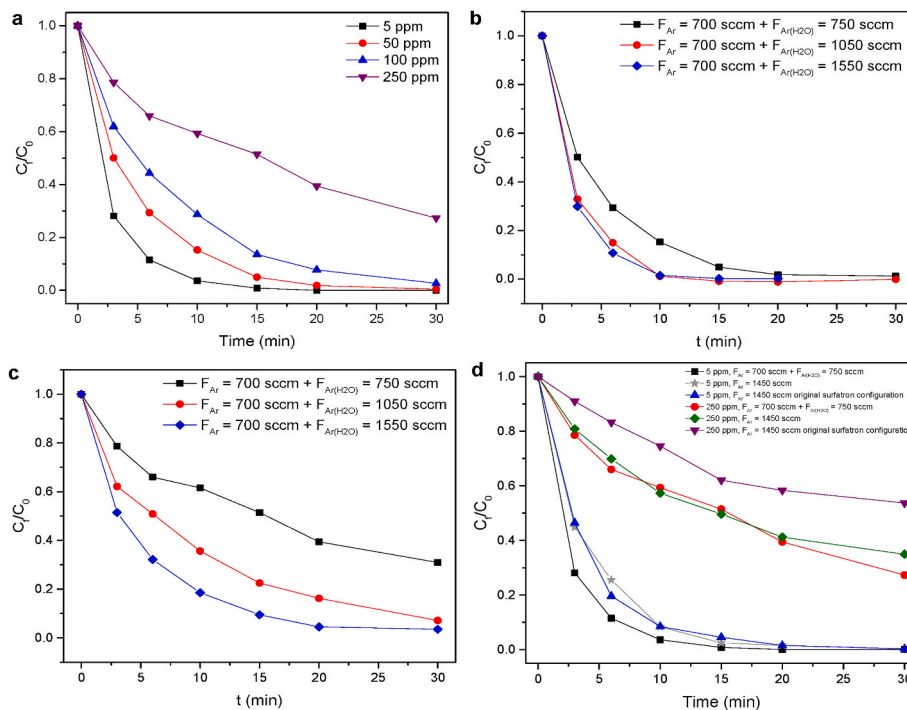

Fig. 5. a. Degradation of the dye over time for plasma treatments of MB aqueous solutions at different initial concentrations by using $F_{Ar} = 700$ sccm and $F_{Ar(H_2O)} = 750$ sccm. Fig. 5b and c. Degradation of the dye over time with MB concentrations of 50 and 250 mg L^{-1}, respectively, for plasma treatments using $F_{Ar} = 700$ sccm and different $F_{Ar(H_2O)}$. Fig. 5d. Evaluation of dye degradation over time with different plasma configurations for MB concentrations of 5 and 250 mg L^{-1}.

absorption intensity at the maxima wavelengths of 291 nm, 616 nm, and 665 nm with increasing treatment duration. Notably, after 15 min of exposure to the plasma, the solution became completely colourless.

The influence of the initial MB concentration in the aqueous solutions on its degradation, operating at $F_{Ar} = 700$ sccm and $F_{Ar(H2O)} = 750$ sccm, is summarized in Table S3, which includes data on kinetic constants, conversion rates, and energy yields. Indeed, Fig. 5a shows that plasma treatment, under these experimental flow rate conditions, provided an extraordinary efficiency in the MB degradation process even at high initial dye concentrations. Conversion rates of 100, 99, 97, and 73% for initial MB concentrations of 5, 50, 100, and 250 mg L^{-1}, respectively, were achieved after 30 min.

Under the conditions tested, the degradation of MB followed a pseudo-first-order kinetics. The apparent kinetic constant, determined from the slope, revealed an increase in the degradation rate as the initial MB concentration decreased. Specifically, the rate improved from 0.0455 min^{-1} at an initial concentration of 250 mg L^{-1} to 0.332 min^{-1} at 5 mg L^{-1}, accompanied by correlation coefficients (R^2) of 0.988 and 0.997, respectively (Table S3). These values far exceed those reported in our previous research (García et al., 2017). Thus, the apparent kinetic constants obtained in the degradation of MB in an aqueous solution with $C_0 = 50$ mg L^{-1} using conventional microwave atmospheric pressure plasma jets in single-tube reactor at an Ar flow rate of 1400 sccm and dual-tube configuration at an Ar flow rate of (700 + 700) sccm were 0.097 and 0.118 min^{-1}, respectively. In the novel surfatron configuration, a value of 0.189 min^{-1} was obtained at the same concentration. Similarly, the MB degradation kinetics exhibited by this new microwave plasma outperformed those of other non-thermal plasma sources (Table 1), including a dielectric barrier discharge plasma reactor (0.119 min^{-1}, $C_0 = 50$ mg L^{-1}) (Manoj Kumar Reddy et al., 2013), an atmospheric pressure non-thermal plasma jet (0.085 min^{-1}, $C_0 = 50$ mg L^{-1}) (Chandana et al., 2015), a high-voltage pulsed Ar gas–liquid discharge plasma (0.043 min^{-1}, $C_0 = 40$ mg L^{-1}) (Yang et al., 2021), a cold-plasma with iron-impregnated spent coffee ground biochar (0.065 min^{-1}, $C_0 = 10$ mg L^{-1}) (Lee et al., 2021) and a multi-needle-to-plane dielectric barrier discharge plasma system (0.060 min^{-1}, $C_0 = 20$ mg L^{-1}) (Zhang et al., 2022).

Compared to other previous investigations reported on dye degradation by plasma treatment (Table 1), this work also demonstrated a notable improvement in degradation kinetics. Specifically, it surpassed the degradation rates achieved by a needle-plate non-thermal plasma reactor operating in argon (0.017 min^{-1}) and air (0.089 min^{-1}) for the degradation of reactive blue 19 (Sun et al., 2016), a pulsed discharge plasma in conjunction with activated carbon for acid orange 7 degradation (0.014 min^{-1}) (Guo et al., 2016), a dielectric barrier discharge plasma used for the degradation of acid orange 7 (Shang et al., 2017) and orange G (Lu et al., 2022) (0.056 and 0.119 min^{-1}, respectively), and a non-thermal plasma generated via corona discharge for acid orange 142 degradation (0.029 min^{-1}) (Fahmy et al., 2020).

Concerning the energy yield, the values obtained at a 50% conversion rate clearly demonstrate the effectiveness of the microwave-induced plasma treatment, even at high dye concentrations. This is a remarkable achievement compared to the results obtained with the microwave-assisted plasma system using the conventional surfatron configuration previously reported by our research group (García et al., 2017). Indeed, at an MB concentration of 250 mg L^{-1}, the energy yield achieved was fourfold, accompanied by a conversion rate that was seven times higher, all while maintaining a comparable total flow rate (ca. 1400 sccm). This suggests that the microwave plasma created in the new surfatron configuration produced reactive species capable of inhibiting interactions among intermediates formed during the plasma treatment (Zhu et al., 2014), which had a direct impact on the MB degradation process.

Conducting a direct comparison between the energy yield reported in this study and those achieved by other non-thermal plasma sources in dye degradation processes is challenging due to the diverse factors that affect its calculation (Eq. (3)), including dye concentration and type, solution volume, power consumption, and gas carrier type and flow rate, among others. The energy yield of the different plasma reactors gathered in Table 1 varies significantly across several orders of magnitude. Restricting our analysis to the degradation of MB solutions, the microwave source proposed in this work generally exhibits a lower

Table 1

Comparison of the kinetic constants and energy yield for dye degradation of different types of plasmas.

Plasma reactor	Dye	C_0 (mg L^{-1})	Flow rate (sscm)	Kinetic constant (min^{-1})	Energy yield (g kWh^{-1})	Ref.
Conventional microwave atmospheric pressure surfatron plasma in single-tube reactor	MB	50	$F_{Ar} = 1440$	0.097	$1.2 \cdot 10^{-2}$	García et al. (2017)
Conventional microwave atmospheric pressure surfatron plasma in dual-tube reactor	MB	50	$F_{Ar} = 700 + F_{Ar} = 700$	0.118	$3.7 \cdot 10^{-2}$	García et al. (2017)
Dielectric barrier discharge non-thermal plasma reactor	MB	50	$F_{air} = 100$	0.119	13.1	Manoj Kumar Reddy et al. (2013)
Atmospheric pressure non-thermal plasma jet	MB	50	$F_{Ar} = 300$	0.085	$4.0 \cdot 10^{-1}$	Chandana et al. (2015)
Double cylindrical dielectric barrier discharge plasma	MB	20	$F_{air} = 3000$	–	$4.2 \cdot 10^{-1}$	Massima Mouele et al. (2020)
High-voltage pulsed Ar gas–liquid discharge plasma	MB	40	$F_{Ar} = 20$	0.043	$4.5 \cdot 10^{-1}$	Yang et al. (2021)
Cold-plasma with iron-impregnated spent coffee ground biochar	MB	10	$F_{air} = 5$	0.065	–	Lee et al. (2021)
Multineedle-to-plane dielectric barrier discharge plasma system	MB	20	–	0.060	$5.4 \cdot 10^{-1}$	Zhang et al. (2022)
		40		0.025	$5.2 \cdot 10^{-2}$	
Needle-plate non-thermal plasma reactor	Reactive blue 19	100	$F_{Ar} = 150$	0.017	2.5	Sun et al. (2016)
			$F_{air} = 150$	0.089	8.0	
Pulsed discharge plasma combined with activated carbon	Acid orange 7	50	$F_{air} = 4000$	0.014	–	Guo et al. (2016)
Dielectric barrier discharge plasma (assisted by persulfate)	Acid orange 7	5	–	0.056	$2.6 \cdot 10^{-4}$	Shang et al. (2017)
Non-thermal plasma generated by corona discharge	Acid Orange 142	20	–	0.029	$1.0 \cdot 10^{-2}$	Fahmy et al. (2020)
Dielectric barrier discharge plasma	Orange G	100	–	0.119	$8.2 \cdot 10^{-2}$	Lu et al. (2022)
Glow discharge electrolysis plasma	Brilliant green	30	–	0.351	$5.9 \cdot 10^{-4}$	Gao et al. (2006)
Modified Surfatron MW (2.45 GHz)	MB	5	$F_{Ar} = 700 + F_{Ar (H2O)} = 750$	0.332	$6.3 \cdot 10^{-3}$	This work
		50		0.189	$4.2 \cdot 10^{-2}$	
		100		0.125	$5.1 \cdot 10^{-2}$	
		250		0.046	$4.0 \cdot 10^{-2}$	

performance in terms of energy yield. However, it should be noted that rather than the actual power absorbed in the plasma (commonly utilized in this determination), the power used in our calculations (105 W) was that delivered by the microwave generator, which is higher due to various losses that cannot be precisely quantified (such as those associated with the heating of coaxial cables and surfatron, as well as radiation).

The impact of the humidified Ar flow rate on the degradation of the MB was also evaluated. Fig. 5b and c depict the degradation of the dye over time, focusing on high MB concentrations (50 and 250 mg L^{-1}), during plasma treatments with varying $F_{Ar(H2O)}$ settings (750, 1050, and 1550 sccm), while keeping F_{Ar} constant at 700 sccm. The kinetic curves demonstrated a faster degradation of the dye at higher $F_{Ar(H2O)}$, owing to the increased number of active plasma species reaching the aqueous solution per unit of time. Moreover, the increase in $F_{Ar(H2O)}$ resulted in higher apparent kinetic constants and conversion rates, as outlined in Table S4. Notably, complete conversion was achieved at $F_{Ar(H2O)} = 1550$ sccm when the initial MB concentration was 50 mg L^{-1}, giving the highest kinetic rate recorded in this study at 0.401 min^{-1} with an exceptionally high R^2 value of 0.999.

Similarly, when operating at constant $F_{Ar(H2O)}$ with the highest initial MB concentration of 250 mg L^{-1}, a conversion of 96% was achieved, obtaining a remarkable kinetic constant of 0.160 min^{-1} in the dye degradation process, supported by a high R^2 value of 0.996. These findings strongly confirm the effectiveness of the plasma setup for treating wastewater with high MB concentrations.

Additionally, an assessment of the plasma efficiency when introducing water into the argon stream ($F_{Ar} = 700 + F_{Ar(H2O)} = 750$) was conducted. This evaluation encompassed MB concentrations of both 5 and 250 mg L^{-1}, as depicted in Fig. 5d. In this way, dye degradation tests were performed using a total argon flow of 1450 sccm, using both the new and the original surfatron configuration, in order to investigate the parameters mentioned earlier. As shown in Table 2, all plasma configurations achieved a complete conversion within 30 min of treatment when the initial dye concentration was 5 mg L^{-1}.

Nonetheless, the most remarkable results in terms of MB degradation kinetics and energy efficiency were obtained when utilizing the novel surfatron configuration in combination with $F_{Ar} = 700$ sccm $+ F_{Ar(H2O)} = 750$ sccm ($k = 0.3316$ min^{-1}, $Y = 0.0063$ g kWh^{-1}). There were no significant differences in some parameters when comparing setups with and without the Si piece for a MB initial concentration of 5 mg L^{-1}. In contrast, significant discrepancies were found when a concentration of 250 mg L^{-1} of MB was employed, as presented in Table 2. In the new configuration, for $F_{Ar} = 1450$ sccm, the use of the silicon piece had a favourable impact, resulting in an enhanced conversion (65%), a faster MB degradation kinetics (0.0408 min^{-1}), and an increased energy yield (0.0405 g kWh^{-1}). These improvements marked a substantial increase when compared to the conventional surfatron configuration without the silicon piece. Furthermore, the incorporation of water in the argon stream ($F_{Ar} = 700 + F_{Ar(H2O)} = 750$) resulted in a more efficient dye degradation, reaching the highest conversion (73%) and kinetic

constant ($k = 0.455$ min^{-1}), all while preserving an optimal energy performance. Improving the efficiency of the new plasma design by using humidified argon is particularly interesting as its potential impact is expected to be even more influential in future applications where the plasma jet does not come into direct contact with an aqueous solution.

4. Conclusions

In this work, a modified design of a surfatron-based reactor was used to sustain non-filamented microwave (2.45 GHz) argon plasmas under atmospheric pressure conditions and using powers from 10 W. This new design also allowed stable maintenance of plasmas with moderate contents of water, enabling the generation of greater quantities of ·OH* species compared to the original surfatron configuration. In terms of electron density and temperature, these plasmas are different from the surface wave-maintained discharges generated in the original configuration, which confirm they do not belong to the same category of MIPs and are most likely better categorized as 'electrode microwave discharges'.

Under the experimental conditions explored in this work (corresponding to relatively high gas flow rates and turbulent regime), it has been demonstrated that both the gas temperature and electron density rise as the fraction of water increases (ranging from 1255 to 1570 K, and from 3.5 to 5.6·10^{20} m^{-3}, respectively). These values are higher than the ones measured using the original surfatron design (960 K and 2·10^{20} m^{-3}). Furthermore, optical emission spectra have unveiled that plasmas containing water can generate relatively high amounts of ·OH* species and H*, which contrasts with pure argon plasmas where the emission is primarily dominated by excited atomic atoms.

Compared to the conventional surfatron setup, the new plasma configuration demonstrated a significant enhancement in the production of peroxides and nitrates when deionized water was treated. Nevertheless, it has been proven that ·OH* precursors involved in hydrogen peroxide formation in the treated liquid mainly come from the dissociation of water molecules evaporated from the sample itself. These discharges were also able to generate nitrates in water, which is likely due to their capability to form NO$_2$ and ·OH precursors at the gas phase.

Finally, the capability of these plasmas to degrade methylene blue (MB) in aqueous solutions was also evaluated. The apparent kinetic constants measured in this study were significantly higher than those reported in our previous work using the conventional surfatron design. Likewise, the MB degradation kinetics presented by this plasma system improved those achieved by other plasma configurations. Concerning the energy yield, the results also evidenced the effectiveness of the plasma treatment even at high dye concentrations. It is worth mentioning that the energy yield obtained at 250 mg L^{-1} MB concentration was fourfold the one in our previous work and also a conversion seven times higher was achieved, while maintaining analogous experimental conditions (total flow rate 1400 sccm, microwave power 105 W).

Table 2

First order kinetic parameters and energy yield at 50% conversion calculated for MB degradation under plasma treatment with different gas flows at 5 and 250 mg L^{-1} of MB.

Concentration of MB (mg L^{-1})	Plasma flow (sscm)	Kinetic constant (min^{-1})	Correlation coefficient (R^2)	Conversion (%)	Energy yield (g kWh^{-1})
5	$F_{Ar} = 700 + F_{Ar(H2O)} = 750$	0.3316	0.997	100	0.0063
5	$F_{Ar} = 1450$	0.2204	0.996	100	0.0044
5	$F_{Ar} = 1450$ original surfatron configuration	0.2066	0.994	100	0.0043
250	$F_{Ar} = 700 + F_{Ar(H2O)} = 750$	0.0455	0.988	73	0.0401
250	$F_{Ar} = 1450$	0.0408	0.970	65	0.0405
250	$F_{Ar} = 1450$ original surfatron configuration	0.0245	0.970	46	0.0182[a]

[a] Maximum value registered (50% conversion was not reached).

Author contributions statement

Juan Amaro-Gahete: Investigation; Methodology; Writing – original draft; and Writing – review & editing; Francisco J. Romero-Salguero: Conceptualization; Funding acquisition; Methodology; Resources; and Writing – review & editing; María C. García: Conceptualization; Data curation; Formal analysis; Funding acquisition; Investigation; Methodology; Resources; Writing – original draft; and Writing – review & editing

Declaration of competing interest

The authors declare that they have no known competing financial interests or personal relationships that could have appeared to influence the work reported in this paper.

Data availability

Data will be made available on request.

Acknowledgments

Appendix A. Supplementary data

Supplementary data to this article can be found online at https://doi.org/10.1016/j.chemosphere.2023.140820.

References

Aggelopoulos, C.A., 2022. Recent advances of cold plasma technology for water and soil remediation: a critical review. Chem. Eng. J. 428, 131657 https://doi.org/10.1016/j.cej.2021.131657.

Britun, N., Gaillard, M., Ricard, A., Kim, Y.M., Kim, K.S., Han, J.G., 2007. Determination of the vibrational, rotational and electron temperatures in N 2 and Ar–N 2 rf discharge. J. Phys. D Appl. Phys. 40, 1022–1029. https://doi.org/10.1088/0022-3727/40/4/016.

Calzada, M.D., Moisan, M., Gamero, A., Sola, A., 1996. Experimental investigation and characterization of the departure from local thermodynamic equilibrium along a surface-wave-sustained discharge at atmospheric pressure. J. Appl. Phys. 80, 46–55. https://doi.org/10.1063/1.362748.

Calzada, M.D., Quintero, M.C., Gamero, A., Cotrino, J., Uría, J.E.S., Sanz-Medel, A., 1992. Determination of bromide by low power surfatron microwave induced plasma after bromine continuous generation. Talanta 39, 341–347. https://doi.org/10.1016/0039-9140(92)80146-5.

Castaños-Martínez, E., Moisan, M., Kabouzi, Y., 2009. Achieving non-contracted and non-filamentary rare-gas tubular discharges at atmospheric pressure. J. Phys. D Appl. Phys. 42, 012003 https://doi.org/10.1088/0022-3727/42/1/012003.

Castaños Martinez, E., Kabouzi, Y., Makasheva, K., Moisan, M., 2004. Modeling of microwave-sustained plasmas at atmospheric pressure with application to discharge contraction. Phys. Rev. E 70, 066405. https://doi.org/10.1103/PhysRevE.70.066405.

Chandana, L., Manoj Kumar Reddy, P., Subrahmanyam, C., 2015. Atmospheric pressure non-thermal plasma jet for the degradation of methylene blue in aqueous medium. Chem. Eng. J. 282, 116–122. https://doi.org/10.1016/j.cej.2015.02.027.

Fahmy, A., El-Zomrawy, A., Saeed, A.M., Z Sayed, A., A Ezz El-Arab, M., Shehata, H., Friedrich, J., 2020. Degradation of organic dye using plasma discharge:

optimization, pH and energy. Plasma Res. Express 2, 015009. https://doi.org/10.1088/2516-1067/ab6703.

Ferreira, C.M., Moisan, M., 1993. Microwave Discharges: Fundamentals and Applications. NATO ASI Series B. Plenum Press, Springer Science & Business Media, New York.

Foster, J., Sommers, B.S., Gucker, S.N., Blankson, I.M., Adamovsky, G., 2012. Perspectives on the interaction of plasmas with liquid water for water purification. IEEE Trans. Plasma Sci. 40, 1311–1323. https://doi.org/10.1109/TPS.2011.2180028.

Foster, J.E., 2017. Plasma-based water purification: challenges and prospects for the future. Phys. Plasmas 24, 55501. https://doi.org/10.1063/1.4977921.

Foster, J.E., Adamovsky, G., Gucker, S.N., Blankson, I.M., 2013. A comparative study of the time-resolved decomposition of methylene blue dye under the action of a nanosecond repetitively pulsed DBD plasma jet using liquid chromatography and spectrophotometry. IEEE Trans. Plasma Sci. 41, 503–512. https://doi.org/10.1109/TPS.2013.2245426.

Foster, J.E., Garcia, M.C., 2022. Promise of nonthermal plasmas in addressing emerging environmental and health problems: present and future. Phys. Plasmas 29, 60601. https://doi.org/10.1063/5.0083766.

Gao, J., Yu, J., Li, Y., He, X., Bo, L., Pu, L., Yang, W., Lu, Q., Yang, Z., 2006. Decoloration of aqueous Brilliant Green by using glow discharge electrolysis. J. Hazard Mater. 137, 431–436. https://doi.org/10.1016/j.jhazmat.2006.02.022.

García, M.C., Mora, M., Esquivel, D., Foster, J.E., Rodero, A., Jiménez-Sanchidrián, C., Romero-Salguero, F.J., 2017. Microwave atmospheric pressure plasma jets for wastewater treatment: degradation of methylene blue as a model dye. Chemosphere 180, 239–246. https://doi.org/10.1016/j.chemosphere.2017.03.126.

García, M.C., Varo, M., Martínez, P., 2010. Excitation of species in an expanded argon microwave plasma at atmospheric pressure. Plasma Chem. Plasma Process. 30, 241–255. https://doi.org/10.1007/s11090-010-9215-x.

García, M.C., Yubero, C., Calzada, M.D., Martínez-Jiménez, M.P., 2005. Spectroscopic characterization of two different microwave (2.45 GHz) induced argon plasmas at atmospheric pressure. Appl. Spectrosc. 59 (4), 519–528, 59, 519–528.

Guo, H., Wang, H., Wu, Q., Zhou, G., Yi, C., 2016. Kinetic analysis of acid orange 7 degradation by pulsed discharge plasma combined with activated carbon and the synergistic mechanism exploration. Chemosphere 159, 221–227. https://doi.org/10.1016/j.chemosphere.2016.05.092.

Hubert, J., Moisan, M., Beauchemin, D., 1986. Spectral and noise characteristics of a xenon microwave-induced plasma lamp. Appl. Spectrosc. 40, 379–385.

Hubert, J., Moisan, M., Ricard, A., 1979. A new microwave plasma at atmospheric pressure. Spectrochim. Acta Part B At. Spectrosc. 34, 1–10. https://doi.org/10.1016/0584-8547(79)80016-6.

Ilias, S., Campillo, C., Borges, C.F.M., Moisan, M., 2000. Diamond coatings deposited on tool materials at a 915 MHz scaled up surface-wave-sustained plasma. Diam. Relat. Mater. 9, 1120–1124. https://doi.org/10.1016/S0925-9635(99)00255-1.

Jin, Q., Zhu, C., Border, M.W., Hieftje, G.M., 1991. A microwave plasma torch assembly for atomic emission spectrometry. Spectrochim. Acta Part B At. Spectrosc. 46, 417–430. https://doi.org/10.1016/0584-8547(91)80039-6.

Kabouzi, Y., Calzada, M.D., Moisan, M., Tran, K.C., Trassy, C., 2002. Radial contraction of microwave-sustained plasma columns at atmospheric pressure. J. Appl. Phys. 91, 1008–1019. https://doi.org/10.1063/1.1425078.

Kabouzi, Y., Moisan, M., Rostaing, J.C., Trassy, C., Guérin, D., Kéroack, D., Zakrzewski, Z., 2003. Abatement of perfluorinated compounds using microwave plasmas at atmospheric pressure. J. Appl. Phys. 93, 9483–9496. https://doi.org/10.1063/1.1574595.

Khan, Idrees, Saeed, K., Zekker, I., Zhang, B., Hendi, A.H., Ahmad, A., Ahmad, S., Zada, N., Ahmad, H., Shah, L.A., Shah, T., Khan, Ibrahim, 2022. Review on methylene blue: its properties, uses, toxicity and photodegradation. Water 14, 242. https://doi.org/10.3390/w14020242.

Lebedev, Y.A., 2015. Microwave discharges at low pressures and peculiarities of the processes in strongly non-uniform plasma. Plasma Sources Sci. Technol. 24, 053001 https://doi.org/10.1088/0963-0252/24/5/053001.

Lee, J.-C., Kim, H.-J., Kim, H.-W., Lim, H., 2021. Iron-impregnated spent coffee ground biochar for enhanced degradation of methylene blue during cold plasma application. J. Ind. Eng. Chem. 98, 383–388. https://doi.org/10.1016/j.jiec.2021.03.026.

Lietz, A.M., Kushner, M.J., 2016. Air plasma treatment of liquid covered tissue: long timescale chemistry. J. Phys. D Appl. Phys. 49, 425204 https://doi.org/10.1088/0022-3727/49/42/425204.

Locke, B.R., Shih, K.-Y., 2011. Review of the methods to form hydrogen peroxide in electrical discharge plasma with liquid water. Plasma Sources Sci. Technol. 20, 034006 https://doi.org/10.1088/0963-0252/20/3/034006.

Lu, P., Boehm, D., Bourke, P., Cullen, P.J., 2017. Achieving reactive species specificity within plasma-activated water through selective generation using air spark and glow discharges. Plasma Process. Polym. 14, 1600207 https://doi.org/10.1002/ppap.201600207.

Lu, W., Sang, W., Jia, D., Zhang, Q., Li, C., Zhang, S., Zhan, C., Mei, L., Li, M., 2022. Improvement of degradation of Orange G in aqueous solution by Fe2+ added in dielectric barrier discharge plasma system. J. Water Process Eng. 47, 102707 https://doi.org/10.1016/j.jwpe.2022.102707.

Lu, X., Naidis, G.V., Laroussi, M., Reuter, S., Graves, D.B., Ostrikov, K., 2016. Reactive species in non-equilibrium atmospheric-pressure plasmas: generation, transport, and biological effects. Phys. Rep. 630, 1–84. https://doi.org/10.1016/j.physrep.2016.03.003.

Machala, Z., Tarabová, B., Sersenová, D., Janda, M., Hensel, K., 2019. Chemical and antibacterial effects of plasma activated water: correlation with gaseous and aqueous reactive oxygen and nitrogen species, plasma sources and air flow conditions. J. Phys. D Appl. Phys. 52, 034002 https://doi.org/10.1088/1361-6463/aae807.

Magureanu, M., Bilea, F., Bradu, C., Hong, D., 2021. A review on non-thermal plasma treatment of water contaminated with antibiotics. J. Hazard Mater. 417, 125481 https://doi.org/10.1016/j.jhazmat.2021.125481.

Manoj Kumar Reddy, P., Rama Raju, B., Karuppiah, J., Linga Reddy, E., Subrahmanyam, C., 2013. Degradation and mineralization of methylene blue by dielectric barrier discharge non-thermal plasma reactor. Chem. Eng. J. 217, 41–47. https://doi.org/10.1016/j.cej.2012.11.116.

Massima Mouele, E.S., Tijani, J.O., Masikini, M., Fatoba, O.O., Eze, C.P., Onwordi, C.T., Zar Myint, M.T., Kyaw, H.H., Al-Sabahi, J., Al-Abri, M., Dobretsov, S., Laatikainen, K., Petrik, L.F., 2020. Spectroscopic measurements of dissolved O3, H2O2 and OH radicals in double cylindrical dielectric barrier discharge technology: treatment of methylene blue dye simulated wastewater. Plasma 3, 59–91. https://doi.org/10.3390/plasma3020007.

Moisan, M., Pelletier, J., 1992. Microwave excited plasmas. In: Plasma Technology. Elsevier, Amsterdam.

Moisan, M., Chaker, M., Zakrzewski, Z., Paraszczak, J., 1987. The waveguide surfatron: a high power surface-wave launcher to sustain large-diameter dense plasma columns. J. Phys. E. 20, 1356–1361. https://doi.org/10.1088/0022-3735/20/11/009.

Moisan, M., Sauve, G., Zakrzewski, Z., Hubert, J., 1994. An atmospheric pressure waveguide-fed microwave plasma torch: the TIA design. Plasma Sources Sci. Technol. 3, 584–592. https://doi.org/10.1088/0963-0252/3/4/016.

Moreau, S., Moisan, M., Tabrizian, M., Barbeau, J., Pelletier, J., Ricard, A., Yahia, L., 2000. Using the flowing afterglow of a plasma to inactivate Bacillus subtilis spores: influence of the operating conditions. J. Appl. Phys. 88, 1166–1174. https://doi.org/10.1063/1.373792.

Nastuta, A.V., Topala, I., Grigoras, C., Pohoata, V., Popa, G., 2011. Stimulation of wound healing by helium atmospheric pressure plasma treatment. J. Phys. D Appl. Phys. 44, 105204 https://doi.org/10.1088/0022-3727/44/10/105204.

NIST, 2023. Atomic Spectra Database Lines Form [WWW Document]. https://physics.nist.gov/PhysRefData/ASD/lines_form.html, 11.1.23.

Oladoye, P.O., Ajiboye, T.O., Omotola, E.O., Oyewola, O.J., 2022. Methylene blue dye: toxicity and potential elimination technology from wastewater. Results Eng. 16, 100678 https://doi.org/10.1016/j.rineng.2022.100678.

Pearse, R.W.B., Gaydon, A.G., 1976. The Identification of Molecular Spectra. Chapman and Hall, London.

Rezaaiyaan, R., Hieftje, G.M., Selby, M., 1987. Spatial emission properties of a surface-wave-sustained plasma (surfatron) in helium. Appl. Spectrosc. 41, 749–761.

Rodero, A., García, M.C., 2017. Gas temperature determination of non-thermal atmospheric plasmas from the collisional broadening of argon atomic emission lines. J. Quant. Spectrosc. Radiat. Transf. 198, 93–103. https://doi.org/10.1016/j.jqsrt.2017.05.004.

Schelz, S., Campillo, C., Moisan, M., 1998. Characterization of diamond films deposited with a 915-MHz scaled-up surface-wave-sustained plasma. Diam. Relat. Mater. 7, 1675–1683. https://doi.org/10.1016/S0925-9635(98)00243-X.

Shang, K., Wang, X., Li, J., Wang, H., Lu, N., Jiang, N., Wu, Y., 2017. Synergetic degradation of Acid Orange 7 (AO7) dye by DBD plasma and persulfate. Chem. Eng. J. 311, 378–384. https://doi.org/10.1016/j.cej.2016.11.103.

Stratton, G.R., Bellona, C.L., Dai, F., Holsen, T.M., Thagard, S.M., 2015. Plasma-based water treatment: conception and application of a new general principle for reactor design. Chem. Eng. J. 273, 543–550. https://doi.org/10.1016/j.cej.2015.03.059.

Sun, Y., Liu, Y., Li, R., Xue, G., Ognier, S., 2016. Degradation of reactive blue 19 by needle-plate non-thermal plasma in different gas atmospheres: kinetics and responsible active species study assisted by CFD calculations. Chemosphere 155, 243–249. https://doi.org/10.1016/j.chemosphere.2016.04.026.

Yang, D.-Z., Zhou, X.-F., Liang, J.-P., Xu, Q.-N., Wang, H.-L., Yang, K., Wang, B., Wang, W.-C., 2021. Degradation of methylene blue in liquid using high-voltage pulsed discharge plasma synergizing iron-based catalyst-activated persulfate. J. Phys. D Appl. Phys. 54, 244002 https://doi.org/10.1088/1361-6463/abecb1.

Yu, Q.S., Yasuda, H.K., 1998. An optical emission study on expanding low-temperature cascade arc plasmas. Plasma Chem. Plasma Process. 18, 461–485. https://doi.org/10.1023/A:1021807215831.

Yubero, C., Calzada, D., C, M., Garcia, M., 2005. Using the Stark broadening of the H α, H β and H γ lines for the measurement of electron density and temperature in a plasma at atmospheric pressure. J. Phys. Soc. Japan 74, 2249–2254. https://doi.org/10.1143/JPSJ.74.2249.

Zhang, X., Shi, P., Zhao, W., Lu, W., Li, F., Min, Y., Xu, Q., 2022. Research on methylene blue degradation based on multineedle-to-plane liquid dielectric barrier discharge mode. Sep. Purif. Technol. 286, 120476 https://doi.org/10.1016/j.seppur.2022.120476.

Zhu, D., Jiang, L., Liu, R., Chen, P., Lang, L., Feng, J., Yuan, S., Zhao, D., 2014. Wire–cylinder dielectric barrier discharge induced degradation of aqueous atrazine. Chemosphere 117, 506–514. https://doi.org/10.1016/j.chemosphere.2014.09.031.